Electrostatic Systems

Abstract This chapter introduces to electrostatic systems used in beam optics, and to the theoretical material needed for the simulation exercises. It begins with a brief reminder of the historical and technological context, and continues with electrostatic optics methods which beam handling, guiding and focusing lean on. `Zgoubi` optical element library offers analytical modeling of several electrostatic components. For instance ELCYLDEF: an electrostatic deflector; ELMULT: a multipole, up to 20 poles; WIENFILTER: a plane condenser, possibly combining a magnetic dipole; ELMIR, ELMIRC: N-electrode mirrors and condenser lenses, with straight or circular slits. Electrostatic elements can be simulated as well using field maps, via the keywords TOSCA, MAP2D-E or ELREVOL. Running a simulation generates a variety of output files, including the execution listing zgoubi.res, always, and, on demand, such files as zgoubi.plt, zgoubi.fai, zgoubi.MATRIX.out, aimed at looking up program execution, storing data for post-treatment such as graphics, etc. Additional keywords are introduced as needed in the exercises, such as the matching procedures FIT[2]; FAISCEAU and FAISTORE to log local particle data in zgoubi.res or in a user defined ancillary file; MARKER; the 'system call' command SYSTEM; REBELOTE do-loop for parameter scans; and some more. This chapter introduces in addition to spin motion in electrostatic fields, the simulation of which is triggered by the keywords SPNTRK. SPNPRT or FAISTORE log spin vector components in respectively zgoubi.res or an ancillary file. The "IL=2" flag logs stepwise particle data, including spin vector, in zgoubi.plt file. Simulations include deriving transport matrix, beam matrix, optical functions, from rays, using MATRIX and TWISS keywords.

DRAFT

Notations used in the Text

A	vector potential
a	gyromagnetic anomaly (electron), $a = 1.15965 \times 10^{-3}$
B	magnetic field
$B\rho$	magnetic rigidity, $B\rho = p/q$
E; m_0c^2; E_i	energy, $E = mc^2$; at rest; injection energy
E; $E_{s,x,y}$	electric field vector; its components in a (O;s,x,y) frame
$E\rho$	electric rigidity. In an electrostatic bend:$E\rho = pv/q$
F	Lorenz force
FOFDOD	a Focusing-drift-Focusing-Defocusing-drift-Defocusing lattice cell
G	gyromagnetic anomaly (hadron). Proton: $G = 1.7928474$
m; m_0	particle mass; at rest
$(O; r, \theta, z)$	cylindrical frame
$(O; s, x, y)$	Cartesin frame
p; $p_{s,x,y}$	momentum vector of a particle; its components
q	particle charge
R_0; r_0	condenser equipotential radii
s	path variable $(*)' = d(*)/ds$
T	kinetic energy
t	time variable $\dot{(*)} = d(*)/dt$
U	potential energy
v; $v_{s,x,y}$	velocity vector of a particle; its components
V; V_i	voltage
Greek symbols	
α	trajectory deflection, $\alpha = \int \frac{E_\perp ds}{E\rho}$
β	v/c
$\delta p/p$; δ	relative momentum offset
ϕ	electrostatic scalar potential
ρ	curvature radius

1.1 Introduction

A well known electrostatic beam line is the column of electrostatic tubes which, in 1932, allowed guiding and accelerating a proton beam to a target reaction, so producing the first artificial atom-splitting, $p + {}^7Li \rightarrow 2\,{}^4He$, the Cockcroft-Walton experiment [1]. A high voltage was produced by an *ad hoc* diode and condenser column rectifying the AC voltage from a transformer. This high DC voltage was applied to a string of conducting cylinders (Fig. 1.1) which ensured beam guiding, (sufficient) focusing, and acceleration to 700 keV, a high enough energy to break the Coulomb barrier in this nuclear reaction. Which earned its authors the 1951 Nobel Prize.

An eventful beam transport in an electrostatic system also: the first acceleration of a polarized proton beam, at the University of Basel in the 1960s, when polarized proton and deuteron sources began operating [3]. The experiment used a 200 keV electrostatic accelerator. "*The Basel group* [...] *presented the first deuteron source*

DRAFT

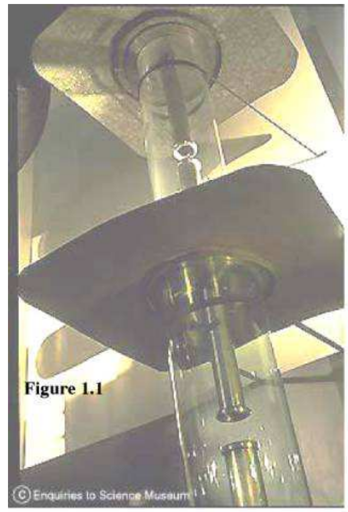

Fig. 1.1 A similar tube cascade to the early 1930s Cockcroft-Walton experiment eponymous acceleration system: Fermilab's 750 keV H^- injector [2]

in operation at the time of the first polarization conference in Basel 1960" [4]. The convention for the sign of polarization is known as the "Basel Convention". Polarized beam acceleration at the nearby ETH Zurich 6 MV Van de Graaff generator was not far behind. Acceleration of polarized ions in nuclear physics cyclic accelerators soon followed, to way higher energy, starting with the cyclotron, a topic addressed in the next chapters.

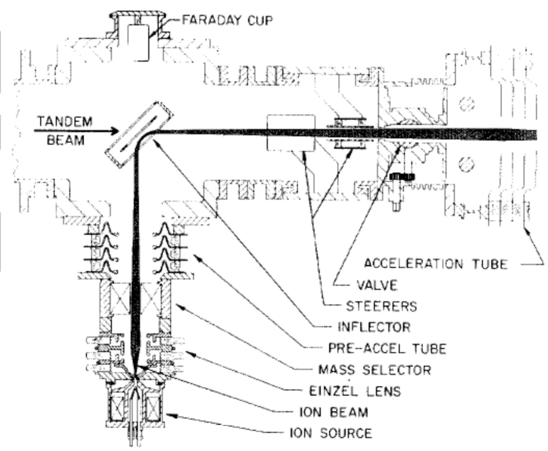

Fig. 1.2 Typical beam handling in an ion source region (BNL AGS injectors). Several electrostatic systems are at work in a short distance: a focusing Einzel lens, a Wien filter mass selector, pre-accelerating tubes, an inflector which serves as a switch with a Tandem ion line, electrostatic condensers to steer the beam, more acceleration tubes

A landmark in physics as well: the electron column. The design of the first electron microscope and of the scanning tunneling microscope earned their authors the 1986 Nobel Prize - well, actually these designs used magnetic lenses.

DRAFT

Nevertheless, the electron column, which combines electrostatic and magnetic components, is a widespread system since, with a number of variants: transmission-, scanning-, photoemission-electron microscope, the electron-beam lithography column, etc. Electron beam energies range in 0.1-1 MeV [5]. A century of design and technological refinements in electron optics, reputedly one of the oldest branches of beam physics, have brought these systems to optical perfection.

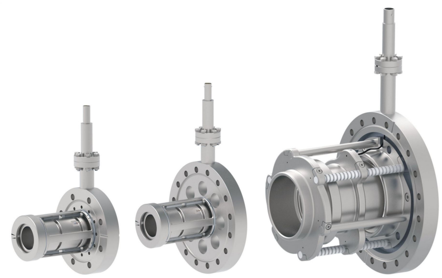

Fig. 1.3 Quite popular, the Einzel lens [6]. Three specimen here, diameters from 10 to 40 mm, operation voltage 10 to 30 kV

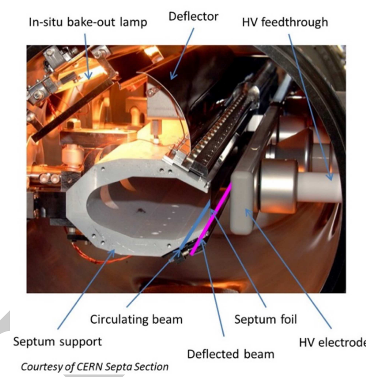

Fig. 1.4 A 250 kV septum for slow extraction from the SPS [7]. Electric field is on the extracted beam side

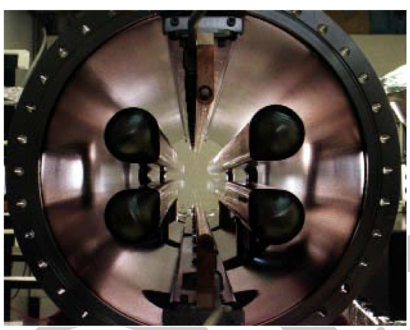

Fig. 1.5 Cornell ESR 3 m long horizontal pretzel separator, operating voltage ±85 kV (2 MV/m). Electrodes are split to let synchrotron radiation through

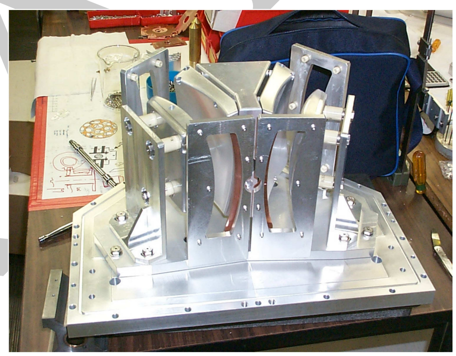

Fig. 1.6 A 3-way spherical electrostatic deflector [8]. Beam can be switched left or right, or let go straight

Electrostatic optical elements present the interest of being light. Deflectors and lenses are simple to construct, simple mechanic forms shape the required fields, electrode voltages can be up to a fraction of a MV, gradients to several MV/m, there is no remanence, power consumption is low. All reasons why electrostatic optical elements are used where energy allows, in low energy beam lines for instance (Fig. 1.2). Guiding and focusing components include prisms, plane condensers, multipoles, mirrors, etc. [11], Figs. 1.3-1.6. Electrostatic components are not a

DRAFT

Fig. 1.7 Elisa in Aarhus, a 25 keV, 7.6 m circumference racetrack for molecular and atomic physics [9]. Its lattice combines spherical deflectors, plane deflectors and quadrupoles

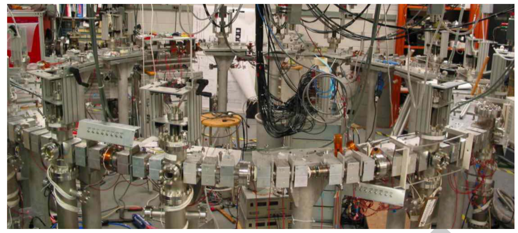

Fig. 1.8 UMER ring at the University of Maryland [10]. A 10 keV, 11.5 m circumference beam optics and beam dynamics test accelerator

specificity of low energy lines though, they span a large range of applications, with energy and size varying accordingly. On the small side are Einzel lenses used in particle source areas (Fig. 1.3). Main bends in beam lines may be of larger volume (Fig. 1.6). Even larger, in the meter range, are injection and extraction septa in GeV synchrotrons (Fig. 1.4), or pretzel orbit separators in GeV e+e- colliders such as LEP and CESR [12, 13] (Fig. 1.5).

The electrostatic septum (Fig. 1.4) in particular is commonly used for beam switching out of or into a circular accelerator. Megavolts/m gradients allow handling high beam rigidities, and achieve fraction of milliradian deflections aimed at. To give an idea of quantities at stake, the septum in Fig. 1.4 for instance is an 80 cm long device here, septum thickness 100 μm, operating voltage 260 kV (15 MV/m over a 17 mm gap) for a deflection angle of 0.28 mrad.

Fig. 1.9 The "Electron Analog", a prof-of-principle of BNL AGS, a strong $n = 225$ index FOFDOD lattice, 45 ft in diameter, built in 1954

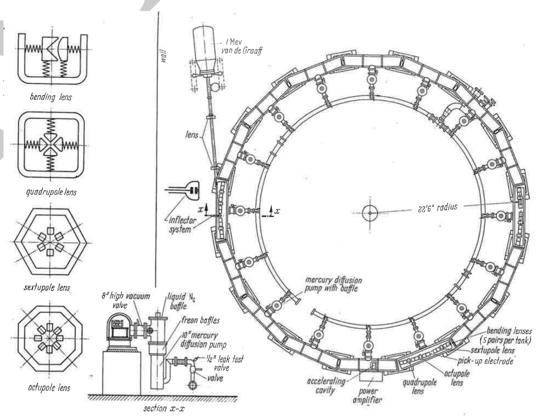

DRAFT

Electrostatic optical elements have also invited themselves in the realm of rings. An electrostatic ring is used every once in a while for proof-of-principle purposes. The first case is the “Electron Analog” (Fig. 1.9), built in 1954 to assess strong focusing and transition-gamma crossing (cf. Chaps. 7, 8), prior to the construction the AGS at the Brookhaven National Laboratory [2]. In the 1990s electrostatic rings were raised to the rank of tools for physics research, with energies of keVs to 10s of keVs. Examples are the ion storage ring ELISA (Fig. 1.7, the beam physics ring UMER (Fig. 1.8), amongst others.

1.2 Basic Concepts and Formulæ

Mathematically speaking, electrostatic elements exploit the scalar potential component in

$$\mathbf{E} = -\mathbf{grad}\phi - \frac{\partial \mathbf{A}}{\partial t}$$

allowing local deflection and/or focusing and/or acceleration along DC voltage gaps. A fundamental aspect is that the resulting Lorentz force works. Particles exchange energy with the field, at a rate $\mathbf{F} \cdot \mathbf{v} = q\mathbf{E} \cdot \mathbf{v}$ which is in general non-zero, thus mass and velocity vary along the trajectory. This is a major difference with magnetic elements, in which $\mathbf{F} \cdot \mathbf{v} = q(\mathbf{v} \times \mathbf{B}) \cdot \mathbf{v} \equiv 0$, the magnetic force does not work, $|\mathbf{v}|$ and mass do not change.

Solving the Lorentz force differential equation $\frac{dm\mathbf{v}}{dt} = q\mathbf{E}$ requires the electric field distribution in space. The latter derives from a potential solution of the Laplace equation $\nabla^2\phi = 0$, The necessary boundary conditions to solve it depend on the electrical properties of the device, on its shape, symmetries, and various components. For instance electrodes are equipotentials to which the electric field is normal; the electric field is along the axis in cylindrical tube; the transverse plane between two identical iso-potential tubes is a symmetry plane, etc. In simple systems, or with some *ad hoc* approximations, it is possible to find an analytical solution to the Laplace equation, from which analytical expressions of the components of the field vector $\mathbf{E} = -\mathbf{grad}\phi$ may be derived. In some complicated cases, it may still be possible to find analytical solutions for field components along a symmetry axis, or over a symmetry plane, and extrapolate from there using Taylor expansion and Maxwell’s equations. With complicated geometry the easiest way may end up being to compute a field map. Raytracing in a field map is at the expense of accuracy of the integration, though, as a result of field interpolation from a mesh. A dense mesh, and an integration step size commensurate with the mesh size may mitigate the issue.

DRAFT

1.2.1 Kinetics

Circular Motion; Rigidity

The Lorentz force on a particle of charge q and mass m in an electric field $\mathbf{E}$ is

$$\mathbf{F} = \frac{d\mathbf{p}}{dt} = \frac{d(m\mathbf{v})}{dt} = q\mathbf{E} \tag{1.1}$$

Circular motion requires velocity $\mathbf{v}$ to be normal to the electric field $\mathbf{E}$. Deflectors allow that, see below. It requires in addition, as in the cyclotron, the centripetal force to equate $\mathbf{F}$. Write it under the form $qE_0 = -mv_0^2/\rho_0$. Forgetting the sign, this yields the electrical rigidity

$$E_0\rho_0 = \ c\beta\,\frac{p_0}{q} = \frac{T}{q}\,\frac{1+\gamma}{\gamma} \tag{1.2}$$

The right hand side is derived introducing the particle kinetic energy $T = mc^2 - m_0c^2$. The trajectory deflection over an arc of length $\int ds$ normally to the field is

$$\alpha = \frac{\int E\,ds}{E_0\rho_0} = \frac{1}{v}\frac{\int E\,ds}{p_0/q} = \frac{1}{v}\frac{\int E\,ds}{(B\rho)} \tag{1.3}$$

where $(B\rho)$ denotes the particle rigidity. The velocity v appears in the expression for the deflection angle, compared to magnetic deflection $\alpha = BL/B\rho$.

Work of the force

The work by a force $\mathbf{F}$ in the time interval t_1, t_2, over $d\mathbf{M} = \mathbf{v}dt$ is

$$\mathcal{T}_{1,2} = \int_{t_1}^{t_2} \mathbf{F}(M,t)d\mathbf{M} \tag{1.4}$$

Developing yields

$$\begin{aligned}\mathcal{T}_{1,2} &= \int_{t_1}^{t_2} \frac{d}{dt}\left(\frac{m_0\mathbf{v}}{(1-v^2/c^2)^{1/2}}\right)\mathbf{v}dt = \int_{t_1}^{t_2} \frac{m_0\mathbf{v}d\mathbf{v}}{(1-v^2/c^2)^{3/2}} \\ &= \int_{t_1}^{t_2} d\left(\frac{m_0c^2}{\sqrt{1-v^2/c^2}}\right) = \int_{t_1}^{t_2} d(mc^2) = [m_2 - m_1]c^2\end{aligned} \tag{1.5}$$

Thus, with kinetic energy defined as $T = mc^2 - m_0c^2 = E - m_0c^2$ the work writes

$$\mathcal{T}_{1,2} = E_2 - E_1 = T_2 - T_1 \tag{1.6}$$

If $\mathbf{F}$ derives from a time-independent potential V, namely $\mathbf{F} = -q\,\mathbf{grad}V(M,\cancel{t})$, then, with $U = qV$,

DRAFT

$$\mathcal{T}_{1,2} = E_2 - E_1 = T_2 - T_1 = -\int_{t_1}^{t_2} \mathbf{grad}U\, d\mathbf{M} = U_2 - U_1 \tag{1.7}$$

thus

$$E_1 + U_1 = E_2 + U_2, \qquad T_1 + U_1 = T_2 + U_2 \tag{1.8}$$

In the non-relativistic limit $v/c \ll 1$, $\gamma \approx 1 + \beta^2/2$ so that, as expected

$$\mathcal{T}_{1,2} = E_2 - E_1 \xrightarrow{\beta\to 0} \frac{1}{2} m_0 (v_2^2 - v_1^2) \tag{1.9}$$

as expected.

Motion in a uniform field

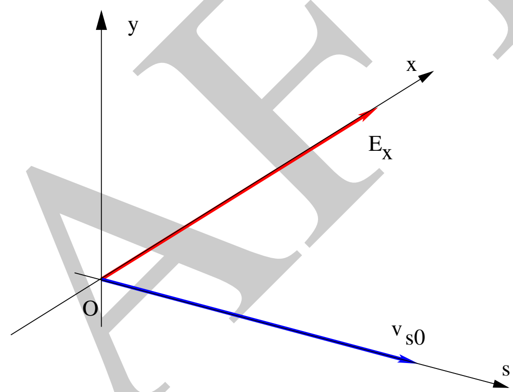

Fig. 1.10 Working frame (O;s,x,y). **E** $\parallel$ **x** and **v**(s = 0) $\parallel$ **s**

Take the x axis parallel to **E**, $\mathbf{E} = E_x\mathbf{x}$. The equations of motion write

$$\frac{d\mathbf{p}}{dt} = q\mathbf{E} \Rightarrow \left| \begin{array}{l} \frac{dp_s}{dt} = 0 \\ \frac{dp_x}{dt} = qE_x \\ \frac{dp_y}{dt} = 0 \end{array} \right. \quad \text{thus} \quad \left| \begin{array}{l} p_s = p_{s0} \\ p_x = qE_x t + p_{x0} \\ p_y = p_{y0} \end{array} \right. \tag{1.10}$$

Simplify the developments by taking the motion parallel to the s axis at time $t = 0$,

$$\mathbf{p}_0 = \left| \begin{array}{l} p_{s0} \\ 0 \\ 0 \end{array} \right. \tag{1.11}$$

Integrating Eq. 1.10 is not straight forward as m is a function of v, such that

DRAFT

$$p_{s,x,y} = \frac{m_0 v_{s,x,y}}{\sqrt{1-\frac{v_s^2+v_x^2+v_y^2}{c^2}}}$$

The difficulty can be surmounted in two steps [15]:

(i) Take $E^2 = p^2c^2 + m_0^2c^4$, with $p^2 = p_s^2 + p_x^2 + p_y^2 = p_{s0}^2 + (qE_xt)^2$, note $E(t=0) = E_i$. Thus

$$E^2(t) = (m_0c^2)^2 + p_{s0}^2c^2 + (qE_xt)^2c^2 = E_i^2 + (qE_xt)^2c^2 \tag{1.12}$$

(ii) With $\mathbf{v} = \mathbf{p}/m = c^2\mathbf{p}/E$, and $p_{s0} = \beta_i E_i/c$ as $\mathbf{p}(t=0) = p_{s0}\mathbf{s}$, one then gets

$$\left|\begin{array}{l} \frac{ds}{dt} = v_s = \frac{p_{s0}c^2}{\sqrt{E_i^2+(qE_xct)^2}} = \frac{\beta_i E_i c}{\sqrt{E_i^2+(qE_xct)^2}} \\ \frac{dx}{dt} = v_x = \frac{qE_xc^2t}{\sqrt{E_i^2+(qE_xct)^2}} \\ \frac{dy}{dt} = v_y = 0 \end{array}\right. \tag{1.13}$$

An interesting result here is that the longitudinal velocity decreases with time. The transverse acceleration causes longitudinal deceleration. v_x increases, with c an upper limit:

$$\frac{dx}{dt} = v_x = \frac{qE_xc^2t}{\sqrt{E_i^2+(qE_xct)^2}} \xrightarrow{t\to\infty} \frac{qE_xc^2t}{\sqrt{(qE_xct)^2}} = \pm c$$

The trajectory slope increases linearly with time,

$$\frac{dx}{ds} = \frac{dx/dt}{ds/dt} = \frac{qE_x}{p_{s0}}t = \frac{qE_xc}{\beta_iE_i}t \tag{1.14}$$

Integrate the differential Eqs. 1.13:

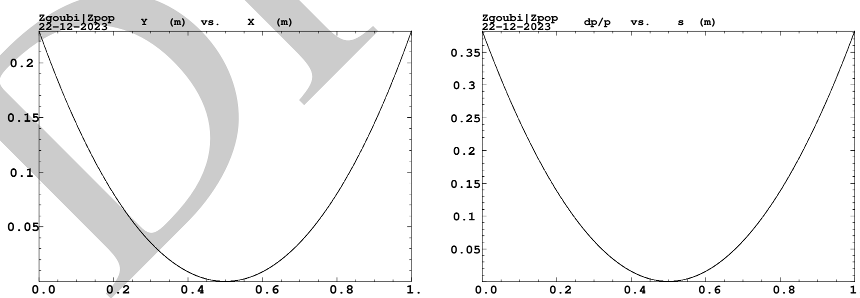

Fig. 1.11 Left: a catenary, trajectory of a 350 keV electron over 1 m in a E_s = 980 kV/m field. Right: the evolution of its relative momentum offset $\delta p/p_0$ from $s=0$ to $s=1$ m (p_0 is taken at maximum momentum, half-way through)

DRAFT

$$\left| \begin{array}{l} ds = \frac{p_{s0}c^2dt}{\sqrt{E_i^2+(qE_xct)^2}} = \frac{p_{s0}c}{qE_x}\frac{dt}{\sqrt{a^2+t^2}}, \quad \text{with } a = \frac{E_i}{qE_xc} \\ dx = \frac{qE_xc^2tdt}{\sqrt{E_i^2+(qE_xct)^2}} = \frac{ctdt}{\sqrt{a^2+t^2}} \\ dy = 0 \end{array} \right. \tag{1.15}$$

On the one hand $\int \frac{dt}{\sqrt{a^2+t^2}} = \text{Asinh}\frac{t}{a}$; on the other hand $\int \frac{tdt}{\sqrt{a^2+t^2}} = \sqrt{a^2+t^2}$, so that

$$\left| \begin{array}{l} s = \frac{p_{s0}c}{qE_x}\int_0^t \frac{dt}{\sqrt{a^2+t^2}} = \frac{p_{s0}c}{qE_x}\left[\text{Asinh}\frac{t}{a}\right]_0^t = \frac{p_{s0}c}{qE_x}\text{Asinh}\frac{qE_xct}{E_i} \\ x = c\int_0^t \frac{tdt}{\sqrt{a^2+t^2}} \quad = c\left[\sqrt{a^2+t^2}\right]_0^t \quad = \frac{1}{qE_x}\left[\sqrt{E_i^2+(qE_xct)^2} - E_i\right] \\ y = 0 \quad \text{(motion is in (O;s,x) plane)} \end{array} \right. \tag{1.16}$$

The trajectory $x(s)$ is obtained by eliminating time between x and s using

$$qE_xct = E_i \sinh\frac{qE_xs}{p_{s0}c} \tag{1.17}$$

so that (accounting for $\cosh^2 - \sinh^2 = 1$)

$$x = \frac{E_i}{qE_x}\left(\cosh\frac{qE_xs}{p_{s0}c} - 1\right) = \frac{E_i}{qE_x}\left(\cosh\frac{qE_xs}{\beta_iE_i} - 1\right) \tag{1.18}$$

The motion is a catenary - the shape of a chain hanging by its two ends, under the effect of gravitation (Fig. 1.11). A paraxial approximation, valid for a small enough deflection, takes the Taylor development of cosh, yielding a parabolic trajectory

$$x_{\text{paraxial}} \approx \frac{1}{2}\frac{qE_x}{\beta_i^2E_i}s^2 \approx \frac{s^2}{2\rho_0} \tag{1.19}$$

where $\rho_0 = \beta_i^2E_i/qE_x$ is the radius of the tangent circle to the parabola.

1.2.2 Optical Components

As a particle travels in the electric field of an electrostatic elements, its energy changes because the field along the path is in general not normal to the velocity, $\mathbf{F}\cdot d\mathbf{M} \neq 0$ in Eq. 1.1. This affects the velocity and mass (Eq. 1.5).

In optical elements a reference optical axis is defined, straight or curved depending on the device. The analytical formalism in general assumes paraxial optics, *i.e.* trajectory angle to the optical axis remains small.

In various optical components, such as the Wien filter (see Sect. 11.2.4), quadrupoles, toroidal deflectors, the electric field is normal to the optical axis. Implications are

DRAFT

- the field is considered normal to trajectories as well, longitudinal velocity component is preserved,

- transverse excursions are small so that energy change can be ignored.

Things are different in cylindrical lenses and mirrors, where the electric field can be near parallel, or far from normal, to trajectories.

These assumptions aimed at allowing simplifying hypotheses for the sake of analytical modeling, do not have to be anyhow as far as numerical integration of the Lorentz equation is concerned.

1.2.2.1 Transverse Fields

Plane Condenser

A plane condenser is a simple concept (Fig. 1.12): a pair of parallel plates, to which a voltage is applied, allowing the deflection of a charged particle beam. The device is used in various optical systems: for beam guiding in low energy beam lines, electron columns and ion rings; for beam switching; in accelerators up to high rigidities for peeling out or switching beams; for orbit separation in high energy e+e- colliders, to mention a few.

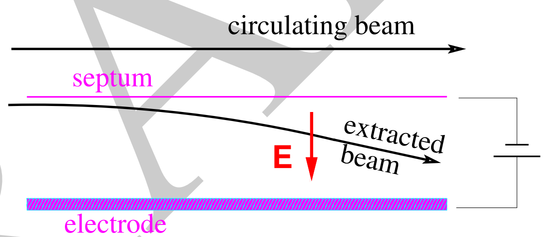

Fig. 1.12 A sketch of a plane condenser used as an electrostatic septum, a separation between a circulating beam, unaffected, and an extracted beam deflected under the effect of the field

The paraxial approximation of the deflection $\alpha \approx \tan\alpha$ undergone over a distance L in the uniform field can be obtained from $\tan\alpha = dx/ds$ (Eq. 1.14), using Eq. 1.17 to remove time, giving

$$\alpha = \frac{qE_x L}{\beta_i p_{s0} c} = \frac{qE_x L}{\beta_i^2 E_i} \tag{1.20}$$

At this point it is interesting to compare with the equivalent effect of a force of magnetic origin, writing $qE = qc\beta B$. Thus,

$$E = c\beta B \quad \text{or} \quad E_{[\mathrm{GV/m}]} \approx 0.3\beta B_{[\mathrm{T}]}$$

A deflection equivalent to that from a 1 T magnetic field, could be achieved with an electric field of 9 MV/m in the case of a $\beta = 0.01$ particle, but is not doable for a $\beta \approx 1$ particle.

DRAFT

The length of the catenary from the origin at (X=0,Y=0) where it is perpendicular to the electric field, to location (X,Y(X)) along the condenser is

$$\begin{aligned} l_{th}(X) &= \int_0^X \left[1 + Y'^2(X)\right]^{1/2} dX \\ &= \int_0^X \left[1 + \left(\frac{1}{\beta_i} \sinh \frac{X}{a}\right)^2\right]^{1/2} dX \ = -ia\, Ei(i\frac{X}{a}, \beta_i^{-2}) \\ &\approx X + \frac{1}{6\beta^2}\frac{X^3}{a^2} + (\frac{1}{3} - \frac{1}{4\beta^2})\frac{1}{10\beta^2}\frac{X^5}{a^4} + \ldots \end{aligned} \tag{1.21}$$

with $Ei(x, k)$ the elliptic integral of the second kind, i the imaginary unit and, to the right, a series approximation.

In the paraxial, parabolic approximation (Eq. 1.19), the radial motion writes [8]

$$x(s) = x_0 + x_0' s + \left[\frac{\delta p}{p}(2 - \beta^2) - 1\right] \frac{s^2}{2\rho_0} \tag{1.22}$$

with s the longitudinal coordinate in the condenser frame (Fig. 1.10).

Toroidal Condenser

A sketch of a toroidal condenser is given in Fig. 1.13, which also defines r_0, the radius of the reference axis and R_0, the vertical curvature radius. The reference axis is in the median plane, along an equipotential $\phi = r_0 E_0/2$ mid-way between the electrodes. This class of electrostatic bend comprises

- spherical condensers, $R_0 = r_0$, electrostatic potential $\phi = E_0 r(\frac{1}{2} - \ln\frac{r}{r_0})$, and
- cylindrical condensers, $1/R_0 = 0$, , electrostatic potential $\phi = Er(\frac{r_0}{r} - \frac{1}{2})$.

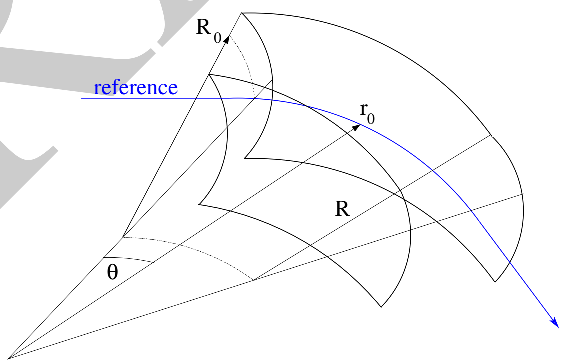

Fig. 1.13 A sketch of an electrostatic bend. A region of radial electric field is defined between concentric electrodes (equipotential surfaces) with axial and radial symmetry. The curvature radius of the reference trajectory $\rho_0 = r_0$

The deflection angle α along the reference axis satisfies Eq. 1.3. The energy of the ideal particle, along the optical axis, satisfies Eq. 1.2. Particle coordinates in a moving frame (see Sect. 2.2.2, Fig. 2.8) can be defined, namely, $x = (r - r_0)$ in the bend plane, y along an axis normal to the latter, and $s = r_0\theta$.

DRAFT

A $\delta p/p$ off-momentum particle differs from the reference one by its mass and velocity. The latter two vary as the particle travels across the bend, exchanging energy with the field. Combine these effects, appropriate approximations lead to the linear equations of motion in a cylindrical condenser ($1/R_0 = 0$) [8]

$$\frac{d^2x}{ds^2} + \frac{2-\beta^2}{\rho_0^2}x = \frac{2-\beta^2}{\rho_0}\frac{\delta p}{p}, \qquad \frac{d^2y}{ds^2} = 0 \tag{1.23}$$

By comparison with the equations of motion in a uniform magnetic field (Eqs. 2.15 taken with a field index $k = 0$), a factor $2-\beta^2$ appears, which tends to 1 at relativistic energy, as $\beta \longrightarrow 1$.

In a toroidal condenser ($r_0/R_0 \neq 0$), in the non-relativistic case ($\beta \approx 0$), the equations of motion in a toroidal condenser write [11]

$$\frac{d^2x}{ds^2} + \frac{2-c}{\rho_0^2}x = \frac{2}{\rho_0}\frac{\delta p}{p}, \qquad \frac{d^2y}{ds^2} + \frac{c}{\rho_0^2}y = 0, \qquad \text{with } c = \frac{r_0}{R_0} \tag{1.24}$$

Quadrupole

With the force parallel to the electric field, transverse focusing requires (in an (x,y) plane transverse to the quadrupole axis)

$$E_x = -Kx = -\frac{\partial\phi}{\partial x}, \qquad E_y = +Ky = -\frac{\partial\phi}{\partial y} \tag{1.25}$$

A '-' sign for E_x is a convention. Thus **E** derives from the scalar potential

$$\phi = \frac{K}{2}(x^2 - y^2) \tag{1.26}$$

In the case of a potential $\pm V/2$ applied at the electrodes, with radius a at pole tip, then $K = -V/a^2$.

The equation of the equipotential is

$$y = \pm\sqrt{x^2 - \frac{2\phi}{K}} \tag{1.27}$$

an hyperbola with its axes at 45 deg to the coordinate axes. As a matter of fact, pause

$$\begin{pmatrix} u \\ v \end{pmatrix} = \begin{pmatrix} \cos 45^\circ & -\sin 45^\circ \\ \sin 45^\circ & \cos 45^\circ \end{pmatrix}\begin{pmatrix} x \\ y \end{pmatrix}, \quad \text{so that } \begin{pmatrix} x \\ y \end{pmatrix} = \begin{pmatrix} \cos 45^\circ & \sin 45^\circ \\ -\sin 45^\circ & \cos 45^\circ \end{pmatrix}\begin{pmatrix} u \\ v \end{pmatrix}$$

In this change of axes, ϕ changes to $\phi^* = Kuv$. Thus, an electrostatic quadrupole skewed by 45 deg achieves the same focusing as a magnetic quadrupole.

The equations of motion have the same form as in a magnetic quadrupole (see Sect. 13.4.2.2), namely

DRAFT

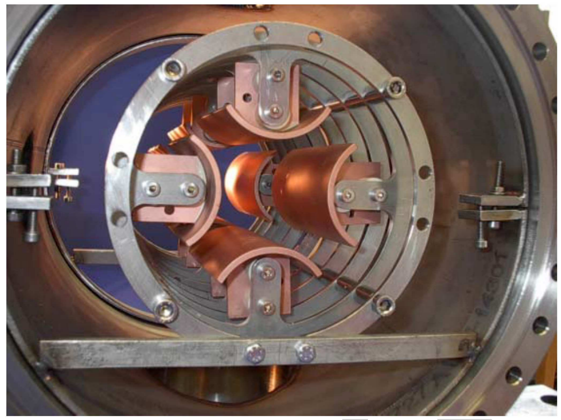

Fig. 1.14 An electrostatic quadrupole [16]. This one, a design for a 50 keV ion ring, operates in the kVolt range

$$\left[\begin{array}{l} \frac{d^2x}{ds^2} + K_x x = 0 \\ \frac{d^2y}{ds^2} + K_y y = 0 \end{array}\right. \qquad \text{with } K_x = -K_y = \frac{-qV}{a^2 m v^2} = \pm \frac{V}{a^2} \underbrace{\frac{1}{|E\rho|}}_{\substack{\text{electric}\\ \text{rigidity}}} \tag{1.28}$$

with the rigidity as defined in Eq. 1.2.

Relative efficiency of an electrostatic quadrupole

From $\mathbf{F} = q\mathbf{E} + q\mathbf{v} \times \mathbf{B}$ one draws the equivalence

$$E = \beta c B \qquad \text{E in V/m, B in T, } c = 3 \times 10^8$$

Technology does allow electric gradients beyond, say, 30 MV/m. For $\beta = 0.1$ this corresponds to $B = 30 \times 10^6/0.1c = 1\,\text{T}$; for $\beta = 1$ this corresponds to $B = 30 \times 10^6/c = 0.1\,\text{T}$. This relative inefficiency limits the use of electrostatic lenses to low energy beam lines.

1.2.2.2 *Electrostatic Mirrors*

Plane condensers include electrostatic mirrors [17]. These devices can be used for strong trajectory deflection, or mirroring. In the latter case the longitudinal component of the velocity cancels, at some location in the particle goes backward.

Sketches of two such devices, available in `Zgoubi` optical element library, are given in Fig. 1.15.

Using the notations defined in Fig. 1.15, potential in the straight slit mirror can be modeled by (after [17])

DRAFT

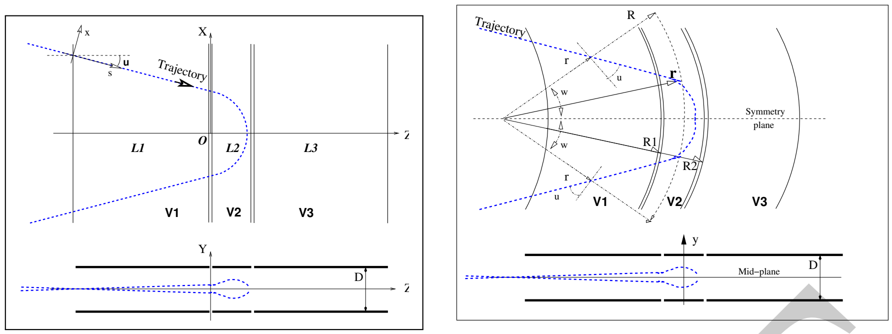

Fig. 1.15 Electrostatic 3-electrode mirror/lens condenser, with straight slits on the left circular slits on the right. Some of the parameters which define these systems: voltages $V_1,\ V_2,\ V_3$, plate lengths (resp. slit radii) $L_1,\ L_2,\ L_3$ $(R_1,\ R_2)$

$$V(z,y) = \sum_{i=2}^{N} \frac{V_i - V_{i-1}}{\pi} \arctan \frac{\sinh(\pi(z - z_{i-1})/D)}{\cos(\pi y/D)} \tag{1.29}$$

This model assumes mid-plane symmetry, and slits of negligible width. The plates are wide enough that $\mathbf{E}$ does not depend on x. N is their number, D is the gap height between plates. The mid-plane field components $E_z(y,z)$ and $E_y(y,z)$ (and derivatives if needed) are obtained by differentiation of $V(z,y)$.

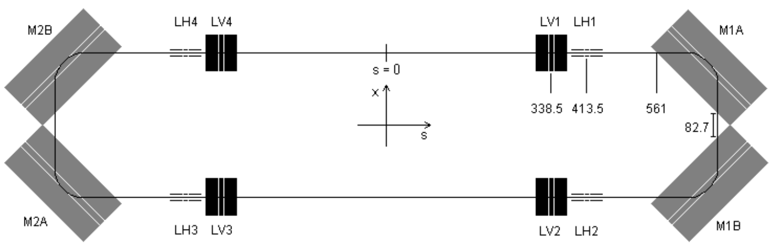

Fig. 1.16 A low energy electrostatic storage ring employed as a multiturn time-of-flight mass spectrometer. Three-plate condensers are used for both focusing (LH1-4, horizontal and LV1-4, vertical) and bending (M1A-B and M2A-B)

The potential of the circular slit mirror can be modeled by

$$V(r) = \sum_{i=2}^{N} \frac{V_i - V_{i-1}}{\pi} \arctan \left(\sinh \frac{\pi(r - R_{i-1})}{D} \right) \tag{1.30}$$

This model assumes mid-plane symmetry, and slits of negligible width. The mid-plane field $E(r)$ (and its r-derivatives if needed) are first derived by differentiation,

DRAFT

then $E(r, y)$ is obtained by Taylor expansion in y, using symmetries and Maxwell relations [18].

An example of a design of a time-of-flight ring for mass separation, based on these optical elements, is displayed in Fig. 1.16. More on this device can be found in [19] and in exercise 1.3.

1.2.2.3 Cylindrical Lenses

Cylindrical lenses are used for their focusing properties, in some cases combined with longitudinal acceleration. Focusing stems from the change of radial velocity through the gap between the tubes. It can be written

$$\Delta v_r = \int_{(\text{gap})} \frac{qE_r(r,z)}{mv_z} dz,$$

with z the longitudinal axis, r the radial coordinate, and assuming revolution symmetry.

Numerical integration of the Lorentz equation along a trajectory only requires knowing the potential. The electric field results, which provides the force which applies on the charged particle. Numerous publications have been dealing with the analytical modeling of cylindrical lenses, and testing these models. Below are a few examples, furthermore found in `zgoubi` optical element library.

Unipotential Lens

A schematic of an unipotential lens is given in Fig. 1.17. Revolution symmetry about the z axis is assumed here. Various models for the electrostatic potential along the

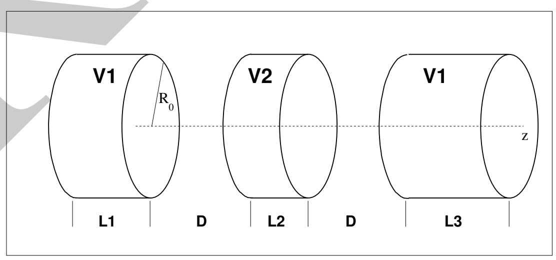

Fig. 1.17 Unipotential lens, with revolution symmetry. The tubes are distant D, they have the same diameter, $2R_0$. Their lengths and potentials are respectively L_1, V_1, L_2, V_2 and L_3, V_1

axis can be found in the literature, not so different anyway. A possibility is [20]

DRAFT

$$V(z) = \frac{V_2 - V_1}{2\omega D}\left[\ln \frac{\cosh \dfrac{\omega\left(x + \dfrac{L_2}{2} + D\right)}{R_0}}{\cosh \dfrac{\omega\left(x + \dfrac{L_2}{2}\right)}{R_0}} + \ln \frac{\cosh \dfrac{\omega\left(x - \dfrac{L_2}{2} - D\right)}{R_0}}{\cosh \dfrac{\omega\left(x - \dfrac{L_2}{2}\right)}{R_0}}\right] \tag{1.31}$$

The origin for z is in the middle of the central lens, and $\omega = 1.318$.

Differentiation of $V(z)$ provides the electrostatic field component $E_z(z)$ along the longitudinal axis. Radial and azimuthal field components along the latter are null. Taylor expansions provide $\mathbf{E}(r, z)$ [18, Sect 1.3.2],

Bipotential Lens

This is the basic optical block of a string of tubes, including multi-gap acceleration columns. An analytical model for the potential in the geometry of Fig. 1.18, in the case where the distance between the two tubes is negligible, is [21, Chap. 5, Sect 5.1.2] [18, *cf.* EL2TUB], r- and θ-independent, namely

$$V(z) = \frac{V_2 - V_1}{2} \tanh \frac{\omega z}{R_0} + \frac{V_1 + V_2}{2} \qquad \text{if } D \to 0 \tag{1.32}$$

The origin for z is half-way between the electrodes, and $\omega = 1.318$.

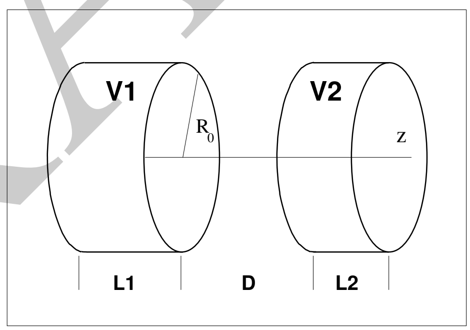

Fig. 1.18 Bipotential lens. The tubes have the same diameter, $2R_0$, their potentials are respectively V_1 and V_2

A second model assumes that the distance D between the two tubes is large enough that the field fall-offs from the two lenses do not overlap. It is written

$$V(z) = \frac{V_2 - V_1}{2} \frac{1}{2\omega D/R_0} \ln \frac{\cosh \omega \dfrac{z + D}{R_0}}{\cosh \omega \dfrac{z - D}{R_0}} + \frac{V_1 + V_2}{2} \qquad \text{if } D > R_0 \tag{1.33}$$

DRAFT

If a string of more than 2 tubes is modeled, an upstream end lens (respectively downstream) is modeled using $V_1 = 0$ (resp. $V_2 = 0$).

Differentiation of $V(z)$ provides the electrostatic field component $E_z(z)$ along the longitudinal axis. Radial and azimuthal field components along the latter are null. Taylor expansions provide $\mathbf{E}(r, z)$ [18, Sect 1.3.2],

1.2.3 Periodic Structures

Periodic electrostatic structures are typically found in rings. ELISA, UMER and the Electron Analog are three examples, respectively Figs. 1.7, 1.8 and 1.9.

In the aforementioned hypotheses of paraxial optics, electric fields normal to the velocity vector, assuming negligible energy exchange between the beam and the electric field, particle motion abides by the principles of betatron motion. Basic theoretical material can be found in Chaps. 2-8. Some insight is gained in the simulation exercises.

These assumptions may however be misleading, acceleration or deceleration in the course of betatron motion may have noticeable effects. Fringe fields may also have affect particle motion. This in addition translates into coupling between transverse and longitudinal motions. Stepwise raytracing is exempt of these limitations, as field models can be made as accurate as necessary, whereas numerical integration accounts for possible energy variation.

These rings are typically synchrotron style of beam instruments. Longitudinal beam handling can use RF systems, for beam bunching, or for acceleration or deceleration. Bend and lens voltages are ramped during acceleration. Note that the latter may in principle be faster than with magnetic optics where eddy currents are a restricting factor. Alternate techniques may be thought of, some of which are addressed in one or the other of the next chapters.

Cyclic Acceleration Using an Electrostatic Field?

Is it possible to accelerate on a closed orbit using a DC voltage? The answer is 'no'.

The work of the force $\mathbf{F} = q\mathbf{E}$ over a path from A to B (top Fig. 1.19). only depends on the initial and final states, $U_A = qV_A$ and $U_B = qV_B$ (Eq. 1.7), it does not dependent on the details of the path. Thus, using an electrostatic field ($\mathbf{E} = -\mathbf{grad}V(\mathbf{R})$) it is not possible to accelerate a particle traveling on a closed path (bottom Fig. 1.19) as $\oint \mathbf{F}.d\mathbf{s} = 0$. As a consequence, a DC voltage gap in a circular machine does not produce energy gain.

DRAFT

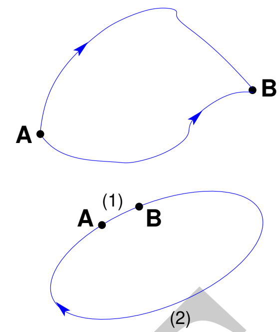

Fig. 1.19 Top: the work of the electrostatic force only depends on voltages at A and B, V_A and V_B, independently of the path. Bottom: case of a closed path, the particle loses along (2) the energy gained along (1).

1.2.4 Spin Precession

Consider the classical model which, to the spin angular momentum $\mathbf{S}$ of a particle of charge q and mass m, associates the magnetic moment $\boldsymbol{\mu} = (1+G)\frac{q}{2m}\mathbf{S}$ of a spinning charge [22, Sect. 2.2]. In that model, under the effect of an ambient magnetic field $\mathbf{B}_a$, $\mathbf{S}$ undergoes a torque

$$\frac{d\mathbf{S}}{dt} = (1+G)\frac{q}{2m}\mathbf{S}\times\mathbf{B}_a \tag{1.34}$$

A particle traveling in the electrostatic field $\mathbf{E}$ of an optical system experiences in its rest frame a magnetic field which is the Lorentz transform of the former (it also experiences a electric field, which does not have any effect on the spin). Expressing the latter in terms of the Lorentz transform of the laboratory field $\mathbf{E}$ yields the differential equation of spin precession,

$$\frac{d\mathbf{S}}{ds} = \mathbf{S}\times\frac{\boldsymbol{\omega}}{B\rho} \tag{1.35}$$

around a precession vector

$$\boldsymbol{\omega} = \gamma\left(a + \frac{1}{1+\gamma}\right)\frac{\mathbf{E}\times\boldsymbol{\beta}}{c} \tag{1.36}$$

In these expressions, $\mathbf{S}$ is in the particle frame, it has not been Lorentz-transformed, and all other quantities, including time, are expressed in a laboratory frame.

1.3 Exercises

1.1 Plane Condenser; Spin Motion

Solution: page 305

DRAFT

Electron dynamics in a parallel plate condenser is considered in this exercise. Use WIENFILTER to simulate it, hard-edge field model.

Take condenser length 1 m, and electric field $|E| = 0.98$ MV/m. Note: the reason for this electric field vaue is to be found in exercise 11.13 et seq., an optimal field setting of a Wien filter used as a spin rotator.

(a) Produce a graph of a symmetric catenary across the condenser.

Check the transverse excursion of a particle and trajectory length, versus theory.

(b) Produce a graph of $(Y_{\mathrm{num}} - Y_{\mathrm{th}})/Y_{\mathrm{th}}$ as a function of integration step size. Y_{num}: particle excursion at the downstream end of the condenser, from numerical integration. Y_{th}: theoretical expectation, Eq. 1.18.

Use REBELOTE[IOPT=1] as a do-loop, changing the integration step size, WIENFILTER[XPAS], at each pass.

(c) Add spin, parallel to the electric field **E** at start. In a similar manner to (b) produce a graph of $(\theta_{\mathrm{num}} - \theta_{\mathrm{th}})/\theta_{\mathrm{th}}$ as a function of integration step size. θ_{num}: spin angle at the downstream end of the condenser, from numerical integration. θ_{th}: theoretical expectation, Eqs. 1.35, 1.36.

For spin tracking, add SPNTRK.

1.2 Toroidal Condenser

Solution: page 307.

Use ELCYLDEF to simulate a toroidal condenser.

(a) Set up a simulation showing that, in the paraxial hypothesis, in a cylindrical condenser, a diverging beam is re-focused after a deflection $\alpha = \pi/\sqrt{2}$.

Test the convergence of the numerical solution versus integration step size.

(b) Produce the aberration curve $Y(T)$ at the focal plane. The moving frame can be shifted to the latter using AUTOREF.

1.3 A Time-of-Flight Mass Spectrometer

Solution: page 309

Multiturn storage is a convenient way to achieve high resolution mass separation, in a compact apparatus. Electrostatic mirrors are potential candidates as both deflector and focusing optical element for a low energy storage ring. The design displayed in Fig. 1.16 is an example. This exercise reviews various of its aspects.

(a) The parameters of the ring are given in Tab. 1.1. Use ELMIR with appropriate MOD option for both focusing lenses (LH, MOD=22 and LV, MOD=21) and bends (MA and MB, MOD=11).

Build `zgoubi` input data file. Produce a synoptic of the ring in laboratory coordinates.

Produce the ring tunes, chromaticities. Produce a graph of the optical functions. TWISS can be used for that.

Produce a graph of horizontal or vertical trajectory over a few tens of turns.

(b) Produce a chromaticity scan (*i.e.*, wave numbers as a function of momentum offset).

(c) Produce 1000-turn horizontal and vertical phase space motion, up to maximum stable amplitudes.

DRAFT

Table 1.1 The parameters of a half-cell of the ring are given, as the cell is symmetric. Referring to Fig. 1.16: this parameter list starts from the center of the long drift ($s = 0$), going clockwise.

particle		N_2
mass	uma	28
mass	GeV	26.082
charge	|e|	1
kinetic energy	keV	400
Geometry:		
ring circumference$^{(a)}$	cm	393.73658
gap height in condensers	m	0.012
number of slits in LH, LV		2
number of slits in M		6
length, electrode lengths:		
drift	(cm)	30.7
LV1	(3×cm)	2.525, 1.25, 2.525
drift		1.2
LH1	(3×cm)	2.525, 1.25, 2.525
drift	(cm)	11.6
M1	(7×cm)	4.275, 5×0.4163, 10
drift	(cm)	6.00217933
electrode voltages, in that order:		
LV1	(V)	0, 115, 0
LH1	(V)	0, 40, 0
M1A	(V)	0, 5×200, 400

(a) This is the length of the reference closed orbit

(d) Produce the time-of-flight histograms after 20 turns, for a bunch comprised of two masses: $M1 = 26.082$ GeV and $1.0004 \times M1$. Both bunches have a 400 keV average energy, *rms* energy spread $\delta E/E = 10^{-4}$, *rms* emittances $\epsilon_x/\pi = 0.02138\ 10^{-6}$ m and $\epsilon_z/\pi = 0.0106\ 10^{-6}$ m. All particles leave from s=0 at the same time.

Use PARTICUL[M=M1,M2] to define two different masses [18, *cf.* PARTICUL].

1.4 The AGS Electron Analog

Solution: page 314

A schematic of the AGS electron analog is given in Fig. 1.9. Its parameters are given in Tab. 1.2. Refer to Chaps 7, 8 for preliminary notions regarding betatron motion.

Table 1.2 Parameters of the AGS electron analog [2]

injection energy, T_i	MeV	1
maximum energy, $E_{\max}$	MeV	10
physical radius, R	feet	22.5
curvature radius, ρ	ft	15
lattice cell		FOFDOD
number of cells, N		40
field index, n		225
phase advance per cell		$\approx \pi/3$

DRAFT

(a) Based on these informations, build a simulation file of the electron analog. Produce a graph of its optical functions.

(b) Accelerate an electron bunch, from 1 to 10 MeV. Produce a graph of the horizontal and vertical phase spaces.

Check the betatron damping, compare with theory.

References

1. Cockcroft, J.D., Walton, E.T.S.: Experiments with High Velocity Positive Ions. Proc. Royal Society of London, A136: 619-630 (1932)
2. Figure 1.1: Credit Reider Hahn, Fermilab
3. Thomas Roser, Anatoli Zelensky, private communication, BNL, June 2021
4. Günther Clausnitzer: History of Polarized Ion Source Developments. In: International Workshop on Polarized Ion Sources and Polarized Gas Jets, February 12-17, 1990, KEK, Tsukuba, Japan. KEK Report 90-15, November 1990, edited by Y. MORI. https://inis.iaea.org/collection/NCLCollectionStore/_Public/22/051/22051667.pdf
5. Wan, W.: Aberration correction in microscopes. TU4PBI02 Proceedings of PAC09, Vancouver, BC, Canada.
6. Figure 1.3: © Dreebit GmbH
7. Paraliev, M., in Proceedings of the CAS-CERN Accelerator School:Beam Injection, Extraction and Transfer, Erice, Italy, 10-19 March 2017, edited by B. Holzer, CERN Yellow Reports: School Proceedings, Vol.5/2018, CERN-2018-008-SP (CERN, Geneva, 2018), pp. 363-394, https://doi.org/10.23730/CYRSP-2018-005.
Figure 1.4: © CERN, 2018. https://creativecommons.org/licenses/by/4.0; no change to the material
8. Bryant, P.J.: Transverse Motion & Electrostatic Elements, Lecture 3. In: Introduction to particle accelerators. Joint Universities Accelerator School, Archamps, 2010.
Figure 1.6: copyrights under license CC-BY-3.0, https://creativecommons.org/licenses/by/3.0; no change to the material
9. Pape Møller, S., et al.: Operational experience with the electrostatic storage ring, ELISA. Proceedings of the 1999 Particle Accelerator Conference, New York, 1999.
https://accelconf.web.cern.ch/p99/PAPERS/WEP16.PDF Figure 1.7: copyrights under license CC-BY-3.0, https://creativecommons.org/licenses/by/3.0; no change to the material
10. Kishek, Rami A., et al.: Benchmarking Space Charge Codes Against UMER Experiments. WEA3MP03 Proceedings ICAP 2006, Chamonix, France
http://accelconf.web.cern.ch/icap06/HTML/AUTHOR.HTM
Figure 1.8: copyrights under license CC-BY-3.0, https://creativecommons.org/licenses/by/3.0; no change to the material
11. Focusing of Charged Particles, Vol. I, II. Academic Press Inc. (1967). Septier, A. Editor
12. W. Kalbreier, N. Garrel, R. Guinard, R.L. Keizer, K.H. Kissler, Layout, Design, and Construction of the Electrostatic Separator System of the LEP e+ e- Collider, Proc. EPAC, vol 2, June 1988, or CERN SPS/88-20 (ABT)
13. Welch, J.J., et al.: Commissioning and performance of low impedance electrostatic separators for high luminosity at CESR. Proceedings of the 1999 Particle Accelerator Conference, New York, 1999.
https://accelconf.web.cern.ch/p99/PAPERS/TUA156.PDF.
Figure 1.3: copyrights under license CC-BY-3.0, https://creativecommons.org/licenses/by/3.0; no change to the material
14. Green, G.K. and Courant, E.E.: The Proton Synchrotron. Part D, Sect. 38, The Electron Analog. In: Handbuch der Physik, Band XLIV, Springer-Verlag, Berlin 1959, p.319.

DRAFT

15. Leleux, G.: Accélérateurs Circulaires. INSTN lectures, Saturne, CEA Saclay, 1978 (unpublished)
16. Welsch, C.P.: Design studies of an electrostatic storage ring. Proceedings of the 2003 Particle Accelerator Conference.
Figure 1.14: copyrights under license CC-BY-3.0,
https://creativecommons.org/licenses/by/3.0; no change to the material
17. S. P. Karetskaya, et al.: Mirror-bank energy analyzers, in Advances in electronics and electron physics, Vol. 89, Acad. Press (1994) 391-491.
18. Méot, F.: Zgoubi Users' Guide.
https://www.osti.gov/biblio/1062013-zgoubi-users-guide.
An up-to-date version of the guide can be found at:
https://sourceforge.net/p/zgoubi/code/HEAD/tree/trunk/guide/Zgoubi.pdf
19. Baril, M., Méot, F., Michaud, D.: Design study of a compact multiturn time of flight mass spectrometer. Internal Report CEA DSM DAPNIA/SEA-00-08 (2008)
20. Septier, A.: *Cours du DEA de physique des particules, optique corpusculaire,* Université d'Orsay, 1966-67, pp. 38-39
21. Galejs, A., Rose, P.H.: Optics of electrostatic tubes. In: Focusing of Charged Particles, Vol. 2, Albert Septier Editor, Academic Press Inc. (1967).
22. Méot, F.: Spin Dynamics. In: Polarized Beam Dynamics and Instrumentation in Particle Accelerators, USPAS Summer 2021 Spin Class Lectures, Springer Nature, Open Access (2023).
https://link.springer.com/book/10.1007/978-3-031-16715-7

DRAFT